Frozen water NMR lineshape analysis enables absolute polarization quantification

Igor Koptyug, Quentin Stern, Sami Jannin, Stuart Elliott

Frozen Water Lineshape Analysis Enables Absolute Polarization Quantification

Stuart J. Elliott[a,b,†], Quentin Stern[a], Igor V. Koptyug[c] and Sami Jannin[a]

[a] Centre de Résonance Magnétique Nucléaire à Très Hauts Champs - FRE 2034 Université de Lyon / CNRS / Université Claude Bernard Lyon 1 / ENS de Lyon, 5 Rue de la Doua, 69100 Villeurbanne, France
[b] Current Address: Department of Chemistry, University of Liverpool, Liverpool L69 7ZD, United Kingdom
[c] International Tomography Center, SB RAS, 3A Institutskaya St., Novosibirsk, 630090 Russia
[†] Stuart.Elliott@liverpool.ac.uk

Abstract

Typical magnetic resonance experiments are routinely limited by weak signal responses. In some cases, the low intrinsic sensitivity can be alleviated by the implementation of hyperpolarization technologies. Dissolution-dynamic nuclear polarization offers a means of hyperpolarizing small molecules. Hyperpolarized water is employed in several dynamic nuclear polarization studies, and hence accurate and rapid quantification of the ^{1}H polarization level is of utmost importance. The solid-state nuclear magnetic resonance spectrum of water acquired under dissolution-dynamic nuclear polarization conditions has revealed lineshapes which become asymmetric at high levels of ^{1}H polarization, which is an interesting fundamental problem in itself, but also complicates data interpretation and can prevent correct estimations of polarization levels achieved. In previous studies, attempts to simulate the ^{1}H spectral lineshape of water as a function of the ^{1}H polarization led to significant disagreement with the experimental results. Here we propose and demonstrate that such simulations, and therefore polarization quantification, can be implemented accurately, in particular by taking into account the detector dead time during ^{1}H signal acquisition that can lead to severe spectral distortions. Based on these findings, we employed an echo-based radiofrequency pulse sequence to achieve distortion-free ^{1}H spectra of hyperpolarized water, and adequate simulations of these echo-based spectra were implemented to extract the absolute ^{1}H polarization level from the hyperpolarized water signal only, thus alleviating the need for lengthy and insensitive measurements of thermal equilibrium signals.

Keywords: NMR, Hyperpolarization, *d*DNP, H_2O, ^{1}H Polarization, Dead Time, Echo Detection, Pake Doublet

1. Introduction

Nuclear magnetic resonance (NMR) spectroscopy and imaging (MRI) experiments are plagued by an intrinsically low sensitivity resulting in weak signals. The low amplitude of NMR and MRI signals can be boosted by up to four orders of magnitude by implementing a variety of hyperpolarization techniques [1], [2]. One such method, dissolution-dynamic nuclear polarization (*d*DNP) [1]–[4], has been employed to strongly polarize nuclear spins in a range of molecules relevant to tumour characterization, ligand-protein binding detection and MRI [5]–[9].

In *d*DNP experiments, the spin system of interest is mixed with a suitable paramagnetic radical species in a solvent formulation which forms a glass when frozen at liquid helium temperature [2]. The DNP sample is irradiated with slightly non-resonant (with respect to the centre of the electron spin transition) microwaves inside a magnetic field, which act to transfer the high thermal equilibrium polarization of the electron spins to the nuclear spins of interest [10]. For nuclear spins with low gyromagnetic ratios, this process is achieved either directly or indirectly; in the latter case by employing nuclear polarization transfer techniques such as cross-polarization (CP) [11]–[15] and its variants [16]–[19].

Water is one of the most ubiquitous substances found on Earth, and has been the target molecule for a number of recent *d*DNP studies [5], [6], [20]–[22]. One remarkable and potentially useful property of H_2O is that it exhibits fundamental nuclear spin isomerism phenomena. Parawater [23], analogous to parahydrogen [24], is a nuclear spin isomer of water in which the spin angular momenta of the two ^{1}H nuclear spins are configured in such a way that the coupled spin state is antisymmetric with respect to permutation of the constituent nuclear spins. The nuclear spin population trapped in the para state of water is not connected to the permutation-symmetric spin states of orthowater and as such can display extraordinary lifetimes under special circumstances [25]. These properties are analogous to the singlet-triplet population imbalance prepared in long-lived state NMR experiments [26].

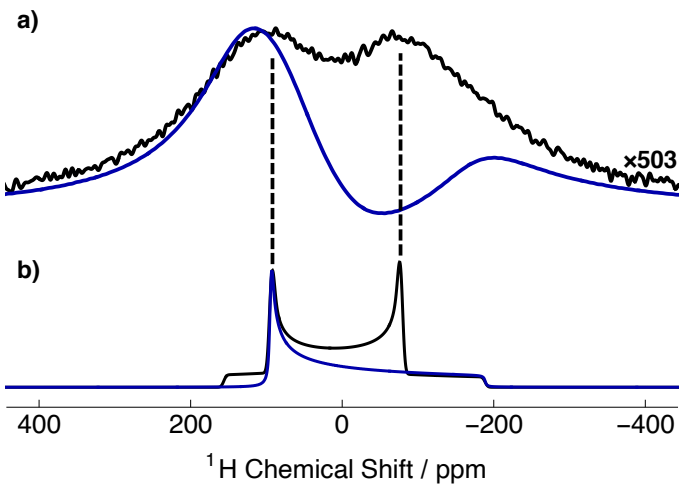

Figure 1: The a) experimental and b) simulated ^{1}H NMR spectra of H_2O in the frozen solid-state under thermal equilibrium (black traces) and DNP conditions (blue traces). As the intensities of the DNP-enhanced spectra are larger by several orders of magnitude than those of their thermal equilibrium counterparts, they are normalized to the intensity of the left Pake horn in each case for convenience. The simulated blue trace corresponds to -100% spin polarization; the experimental polarization value was estimated as -67.5%. Note that the separation of the peaks in the blue experimental trace is measurably larger than the separation of

the Pake horns in the thermal equilibrium spectra. Line broadening was not applied to the simulated ^{1}H NMR spectra.

An earlier attempt of Mammoli et al. in 2015 [27] to prepare water enriched in the ortho spin isomer used DNP to over-populate the permutation-symmetric state manifold. Despite the achieved progress, a few questions remain regarding the behaviour of water under DNP conditions. To illustrate this, Figure 1 presents the experimental and simulated ^{1}H NMR spectra of water at different spin polarization levels in the frozen solid-state. In this case, there are striking traits in the ^{1}H NMR spectra of hyperpolarized water which are unexpected. The simulated spectrum at thermal equilibrium is almost symmetric, as expected (Figure 1b, black trace). It consists of two approximately mirror-image halves, each comprised of a pronounced Pake "horn" with a one-sided broad shoulder (Figure 1b, blue trace and its mirror image). As the polarization level increases, one of these two halves is expected to significantly grow in intensity, while the other gradually diminishes and at 100% polarization disappears completely, so that only one Pake horn remains in the pattern (1b, blue trace).

The experimental spectra, however, seem to tell a different story (Figure 1a). In the spectrum acquired without DNP enhancement (Figure 1a, black trace), the relative intensities and the separation of the two peaks match those in the simulated spectrum (Figure 1b, black trace), which is seen clearly despite the substantial broadening of the experimental spectrum (see below). The spectrum detected under DNP conditions (Figure 1a, blue trace) shows two clear peaks of unequal intensity, apparently indicating a rather high polarization level achieved in the experiment. However, the separation of the two peaks in this DNP-enhanced spectrum is considerably larger than the separation between the horns of the Pake pattern under thermal equilibrium conditions (Figure 1a, black trace). This peak splitting is also considerably larger than predicted by lineshape simulations. Similar issues are apparent in the results reported by Mammoli et al. [27]. These complications make quantification of the ^{1}H polarization from lineshape polarimetry a difficult task, and indeed a value for the ^{1}H polarization was not reported in Reference [27].

In this Communication, we aim to explain these observations by considering the potential underlying mechanisms, and propose that these discrepancies are a direct result of the spectrometer dead time, which is known to engender spectral distortions in a number of cases [28], [29]. To demonstrate this, we recorded experimental pulse-acquire ^{1}H NMR spectra for various levels of proton spin polarization which incorporate the distortion effects engendered by the presence of a dead time. We show that the dead time deleteriously distorts the ^{1}H NMR spectra at high levels of proton spin polarization, so much so that it results in the emergence of false peaks in the spectral patterns and causes an apparent increase of the Pake horn splitting at higher ^{1}H spin polarizations. We further demonstrate that acquisition of an echo signal instead of a free induction decay (FID) can largely eliminate these undesired dead time phenomena and produce distortionless spectra. This allowed us to estimate a ^{1}H spin polarization of ca. -75% after ~34 minutes of proton DNP at 1.2 K from the comparison of the experimental echo-based ^{1}H NMR spectra with their simulations.

2. Methods

2.1. Sample Preparation

A liquid glass-forming mixture of H_2O/DMSO-d_6 (1/5 *v*/*v*) was doped with 50 mM TEMPOL radical (all compounds purchased from *Sigma-Aldrich*) and sonicated for ~2 minutes. This sample is referred to as **I** from here onwards. The concentration of water protons was ~9.25 M. DMSO-d_6 was chosen over glycerol-d_8 due to the wider availability of ~100% deuterated DMSO-d_6 products. The deuteration level of DMSO-d_6 used in experiments was 99.96%, which indicates a residual DMSO-d_6 proton concentration of ~44 mM. Consequently, only ~0.5% of ^{1}H spins belong to the glassing agent and as such the ^{1}H NMR signal observed largely originates from that of water. Lower ratios of H_2O/DMSO-d_6 did not result in a glassy sample upon freezing [30] (see the Electronic Supporting Information (ESI) for more details).

2.2. Sample Freezing

A 20 μL volume of sample **I** was pipetted into a Kel-F sample cup and inserted into a 7.05 T prototype *Bruker Biospin* polarizer equipped with a specialized *d*DNP probe (including a background-free *rf*-coil insert [31]) and running *TopSpin 3.7* software. The sample temperature was reduced to 1.2 K by submerging the sample in liquid helium and reducing the pressure of the variable temperature insert (VTI) towards ~0.7 mbar.

2.3. Dynamic Nuclear Polarization

Sample **I** was polarized by applying microwave irradiation at 198.256 GHz (negative lobe of the DNP enhancement profile) using triangular frequency modulation with amplitude Δf_{mw} = 200 MHz [32] and rate f_{mod} = 0.5 kHz at a power of ca. 100 mW at the output of the microwave source and ca. 30 mW reaching the DNP cavity (power measurement procedure described in Reference [33]), which were optimized by using sample **I** prior to commencing experiments in order to achieve the highest possible level of ^{1}H polarization.

2.4. Pulse-Acquire RF-Pulse Sequence

The build-up of the emissive (negative) DNP-enhanced ^{1}H NMR signal as a function of microwave irradiation time for sample **I** was monitored by using the following protocol (see Figure 2a):

(*i*) A saturation sequence of 90° *rf*-pulses with alternating phases separated by a short delay repeated *n* times (typ. *n* = 50) destroys residual magnetization on the proton *rf*-channel;

(*ii*) The microwave source becomes active permitting ^{1}H DNP;

(*iii*) During microwave irradiation of the sample a small flip angle *rf*-pulse (typ. 0.1°) foments acquisition of the ^{1}H NMR signal;

(*iv*) An irreducible nominal spectrometer dead time (typ. 5 μs at minimum) is included before signal detection;

(*v*) Stages *iii*-*iv* are repeated *i* times (typ. *i* = 64), *i.e.*, 64 FIDs are summed together, often for signal averaging purposes, which leads to a negligible ^{1}H polarization depletion of less than 0.01%;

(*vi*) A waiting period t_{WAIT} is added such that DNP is allowed for a time t_{DNP} (typ. t_{DNP} = 2 s) during each repetition;

(*vii*) Stages *iii*-*vi* are repeated *m* times to record ^{1}H NMR signals between short time intervals.

The implementation of small flip angle *rf*-pulses in low temperature experiments has previously unveiled asymmetries in NMR spectra [27], [34]–[37]. During the DNP build-up time, small flip angle *rf*-pulses are necessary to monitor the ^{1}H hyperpolarization without measurably diminishing it [38], [39]. The proton NMR signal is continuously monitored until a plateau in the signal intensity is reached. The integral of the DNP-enhanced ^{1}H NMR signal is compared with the corresponding proton signal acquired under thermal equilibrium conditions to calculate the signal enhancement considering the number of transients and receiver gain used in individual experiments.

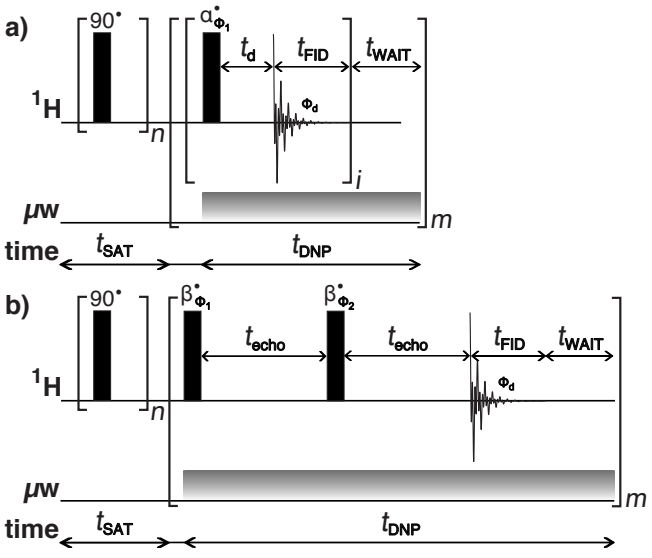

Figure 2: Schematic representations of the a) pulse-acquire and b) echo-based *rf*-pulse sequences used for recording ^{1}H NMR spectra of sample I. The experiments used the following parameters: n = 50; α_{ϕ_1} = 0.1°; t_d = 5 μs (nominal value); i = 64; $\beta_{\phi_1} = \beta_{\phi_2}$ = 10°; $\phi_1 = \phi_2 = y$; t_{echo} = 35 μs; $\phi_d = x$; and t_{DNP} = a) 2 s and b) 15 s. The π/2 saturation *rf*-pulses use an empirically optimized thirteen-step phase cycle to remove residual magnetization at the beginning of each experiment: {0, π/18, 5π/18, π/2, 4π/9, 5π/18, 8π/9, π, 10π/9, 13π/9, π/18, 5π/3, 35π/18}. The resonance offset was placed at the centre of the ^{1}H NMR peak.

2.5. Echo-Based RF-Pulse Sequence

Figure 2b depicts the small flip angle echo-based *rf*-pulse sequence implemented to reduce the influence of artefacts in the experimental ^{1}H NMR spectra of sample **I**. The echo-based *rf*-pulse sequence operates as follows:

(*i* & *ii*) Stages *i* and *ii* are identical to those in Section 2.4;

(*iii*) A solid-echo unit ($\beta_{\phi_1} - \tau_{echo} - \beta_{\phi_2} - \tau_{echo}$) using small flip angle *rf*-pulses (typ. 10°) alleviates the necessity of including a deleterious spectrometer dead time;

(i*v*) A waiting period t_{WAIT} is added such that DNP is allowed for a time (typ. t_{DNP} = 15 s) during each repetition;

(*v*) Stages *iii*-*v* are repeated m times to acquire echo-based ^{1}H NMR signals as a function of $m \times t_{DNP}$, *i.e.*, the microwave irradiation time.

Echo-detection has previously been demonstrated to acquire undistorted lineshapes in experimental solid-state NMR, primarily to remove distortions attributed to the acoustic ringing of the *rf*-coil [40], [41], [42]. The choice of a "plastic-free" *d*DNP *rf*-coil support [31] removes unwanted background proton NMR signals from *rf*-probe materials, which are often deleterious when quantifying ^{1}H spin polarizations. Although small flip angle echo-detection schemes do not allow for complete refocusing of dipolar and chemical shift anisotropy (CSA) interactions, which engender minor spectral artefacts, relatively undistorted experimental ^{1}H NMR lineshapes are produced.

A derivation for the dependence of the signal intensity of an echo-based NMR spectrum on the *rf*-pulse flip angle β_{ϕ_2} in the presence of the two-step phase cycle of the second *rf*-pulse is presented in the ESI. The NMR signal intensity I_{echo} of the echo-based *rf*-pulse sequence is proportional to $\sin(\beta_{\phi_1})\sin^2(\beta_{\phi_2})$, where β_{ϕ_1} and β_{ϕ_2} are the flip angles of the first and second *rf*-pulses in the echo-based sequence, respectively. In the case of $\beta_{\phi_1} = \beta_{\phi_2} = \beta$, the NMR signal becomes proportional to the third power of $\sin(\beta)$. In the small-angle limit when $\tan(\beta) \simeq \beta$, a decrease in the *rf*-pulse flip angle by a factor of 2 would reduce the intensity of the observable NMR signal by a factor of ~8. This motivates the choice of $\beta_{\phi_1} = \beta_{\phi_2}$ = 10°, since this flip angle is sufficiently large to acquire ^{1}H NMR signals with satisfactory signal-to-noise ratios (SNRs) but is significantly smaller than 90° such that major spectral shape distortions are avoided. Moreover, such *rf*-pulses do not substantially diminish the ^{1}H hyperpolarization, *e.g.*, if β = 10° then $\cos(\beta)^2 \simeq 0.97$ and only ~3% of the ^{1}H NMR signal is depleted, so there is no need to implement time consuming experiments in which the sample needs to be repolarized multiple times.

3. Results

The experimental ^{1}H polarization $|P_H|$ build-up curve for sample **I** as a function of the microwave irradiation time is shown in the ESI. Sample **I** polarizes to $P_H \simeq$ -67.5% (see Figure 1) within ~34 min of ^{1}H DNP at 1.2 K with a build-up time constant of $\langle \tau_{DNP}^{-} \rangle$ = 196.7 ± 0.9 s. It is worth noting that the value of $P_H \simeq$ -67.5% was extracted from the pulse-acquire ^{1}H NMR spectra, which are deleteriously distorted by the spectrometer dead time.

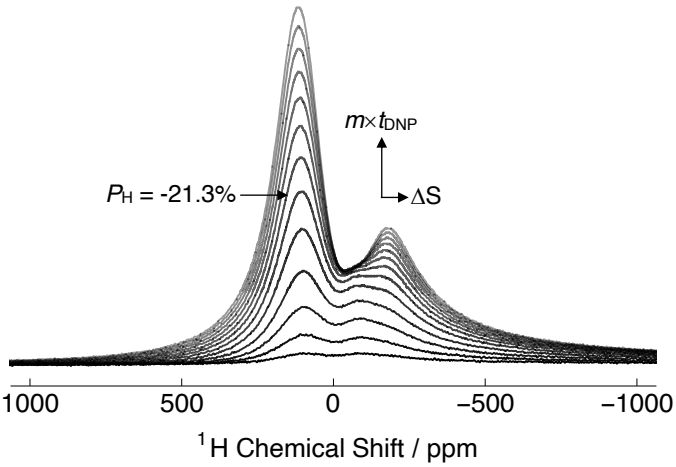

Figure 3: Relevant portion of the experimental pulse-acquire ^{1}H NMR spectra of sample I acquired at 7.05 T (^{1}H nuclear Larmor frequency = 300.13 MHz) and 1.2 K with 64 scans (α_{ϕ_1} = 0.1°; t_d = 5 μs) as a function of the time $m \times t_{DNP}$ for the case of microwave irradiation at the negative lobe of the DNP enhancement profile. Experimental spectra were obtained by implementing the *rf*-pulse sequence depicted in Figure 2a.

Figure 3 shows a series of pulse-acquire ^{1}H NMR spectra for sample **I** acquired during the build-up of proton signal intensity at m intervals of the DNP time (t_{DNP} = 2 s). The SNR is sufficient in all experiments such that a striking asymmetry

is readily observed between the intensities of the two most intense peaks at nearly all time points during the ^{1}H signal build-up, including at relatively small values of m (lower ^{1}H polarizations) where a conventional Pake doublet is observed.

As the ^{1}H NMR signal intensity grows, the asymmetry becomes greater. In the case of the most intense ^{1}H NMR spectrum shown in Figure 3, the rightmost peak of the Pake pattern is ~0.38 the intensity of the leftmost horn. The experimental ^{1}H spin polarization of this spectrum is -38.2%, which was calculated by comparing the hyperpolarized proton NMR spectrum integral with the integral of a thermal equilibrium ^{1}H NMR spectrum acquired at 3.8 K.

Interestingly, the observed splitting between the peaks of the Pake pattern ΔS increases with the proton NMR signal intensity, *i.e.,* ^{1}H spin polarization. This value is extracted from the ^{1}H NMR spectra of frozen water as a function of ^{1}H polarization by fitting the lineshapes to two Lorentzian peaks and calculating the frequency difference between the centre of the two peaks. In the case of the least intense ^{1}H NMR spectrum shown in Figure 3, the peak splitting between the horns of the Pake pattern is ~209.6 ppm. However, the peak splitting ΔS, in the case of the most intense ^{1}H NMR spectrum shown in Figure 3, has grown to ~316.4 ppm (an increase in frequency separation by a factor of ~1.51). This increase in the peak splitting is clearly seen by careful examination of the ^{1}H NMR spectra in Figure 3 (see the ESI for more details). Initially, the imbalance in intensity is between the two horns of the Pake doublet, but once a sufficient level of ^{1}H polarization is reached (-21.3%) a false peak has evidently emerged and creates a larger value of the peak splitting (see Figure 3).

Figure 4 shows an assemblage of echo-based ^{1}H NMR spectra for sample **I** acquired during the microwave irradiation time with sufficient SNR. Nearly all spectra show an asymmetry with respect to the relative intensity of the two Pake horns. As with the pulse-acquire ^{1}H NMR spectra (Figure 3), the asymmetry grows with an increasing proton spin polarization.

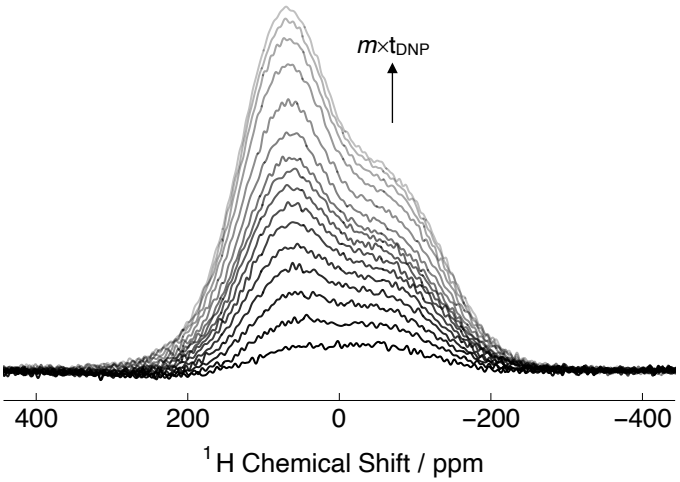

Figure 4: Relevant portion of the experimental echo-based ^{1}H NMR spectra of sample I acquired at 7.05 T (^{1}H nuclear Larmor frequency = 300.13 MHz) and 1.2 K with a single transient ($\beta_{\Phi_1} = \beta_{\Phi_2} = 10°$; t_{echo} = 35 μs) as a function of the time $m \times t_{DNP}$ for the case of microwave irradiation at the negative lobe of the DNP enhancement profile. Experimental spectra were obtained by implementing the *rf*-pulse sequence depicted in Figure 2b.

A striking difference compared with Figure 3 is the relatively constant peak splitting between the horns of the Pake doublet as a function of the ^{1}H polarization level, indicated by the approximately similar lineshapes of the echo-based ^{1}H NMR spectra shown in Figure 4. As demonstrated by lineshape simulations below, this result is due to the incorporation of the dead time into the echo delay, which removes this source of NMR lineshape distortion. The influence of the spectrometer dead time is demonstrated for a pulse-acquire NMR spectrum in the ESI.

The pulse-acquire and echo-based ^{1}H NMR spectra of sample **I** were simulated by using the NMR software package *SIMPSON* [43]. The simulations were performed for a homonuclear 2-spin-1/2 system with: (*i*) a ^{1}H-^{1}H dipolar coupling ($\omega_{HH}/2\pi$ = -34.5 kHz); (*ii*) ^{1}H CSA (σ_{aniso} = -16.19 ppm); and (*iii*) ^{1}H CSA biaxiality (η = 0.17) [27]. The CSA interaction assumes the principal axis is aligned along the OH bond vectors. A powder average over 4181 crystallites (sampling scheme = ZCW4181 [44]) was considered. The initial spin density operator is given by: $\hat{\rho}_0 = (\hat{E} + 2p_H\hat{I}_{1z} + 2p_H\hat{I}_{2z} + 4p_H^2\hat{I}_{1z} \cdot \hat{I}_{2z})/4$, where $\hat{E}$ is the identity operator, p_H is the ^{1}H spin polarization level and $\hat{I}_{iz}$ is the z-angular momentum operator for spin i. $\hat{\rho}_0$ corresponds to a spin density operator for a strongly polarized spin system. Relaxation was not included in the simulation.

Figure 5 displays the simulated echo-based ^{1}H NMR spectra as a function of the ^{1}H spin polarization P_H. Echo-based ^{1}H NMR spectra were simulated by including $p = 0 \rightarrow p = +1 \rightarrow p = -1$ coherence pathway selection to refocus shielding interactions that would otherwise result in distorted spectra [45]. It is readily evident that only two peaks contribute to the ^{1}H NMR lineshape at all ^{1}H spin polarization levels when using the echo-based *rf*-pulse sequence (see Figure 2b). This is due to the echo-compensation of the spectrometer dead time. The simulated echo-based spectra also become increasingly asymmetrical with increased ^{1}H polarizations P_H, as was the case for the experimental echo-detected spectra.

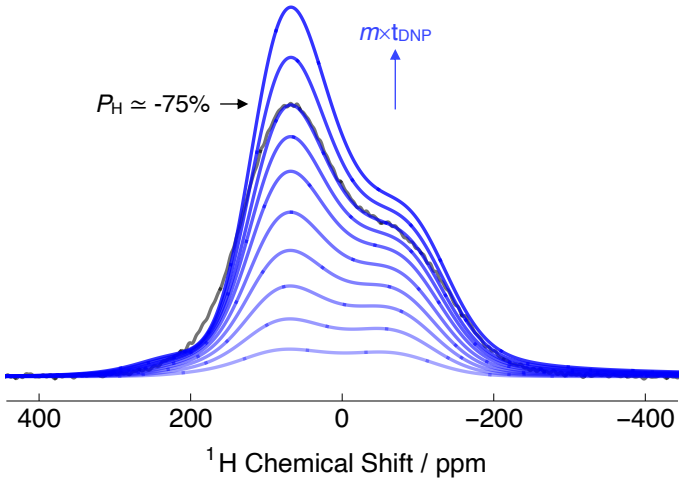

Figure 5: Simulated echo-based ^{1}H NMR spectra ($\beta_{\Phi_1} = \beta_{\Phi_2} = 10°$; t_{echo} = 35 μs) as a function of the ^{1}H polarization level P_H. Black: Experimental spectrum (with $P_H \simeq$ -75%). Gaussian line broadening with full-width at half-maximum height (FWHM) = 30 kHz.

The ^{1}H NMR lineshapes of the echo-based spectra are not dramatically altered by the level of ^{1}H spin polarization, other than their overall intensity. As a result, it is necessary to simulate the echo-based NMR spectra to extract the true ^{1}H polarization level. The black lineshape in Figure 5 is

representative of one of the most intense echo-based spectra in Figure 4 acquired with the experiment presented in Figure 2b. A simulated lineshape corresponding to P_H = -75% fits the experimental spectrum well (see Figure 5). It is a difficult task to compare the hyperpolarized echo-detected ^{1}H NMR spectrum with its thermal equilibrium counterpart since the SNR from using only a 20 μL sample volume is insufficient for ^{1}H polarization quantification with high accuracy. Simulations of pulse-acquire spectra are reported in the ESI.

4. Discussion

It is well-known that the dominant dipolar coupling constant, in this case, from the ^{1}H-^{1}H dipolar coupling, governs the peak splitting between the two horns of a resolved Pake pattern [46]; however, the polarization level of a spin system does not alter the physical internuclear distances and dipolar coupling constants between nuclear spins within the same molecule. The true cause of the spectral artefacts shown in Figure 3 is the inclusion of a detector dead time between the *rf*-pulse and the start of FID acquisition, which gives rise to the misleading observation that the peak splitting between the horns of the Pake doublet increases as a function of the ^{1}H spin polarization. The conventional peak splitting between the Pake pattern horns is $3/2 \times \omega_{ij/HH}/2\pi$ (ca. 46.2 kHz) [46]. However, this assumption is only borne out at very low ^{1}H spin polarization levels close to those of thermal equilibrium. The hyperpolarization experiments indicate a splitting on the order of $\sim 5/2 \times \omega_{HH}/2\pi$ (ca. 88.8 kHz) for the case of highly polarized H_2O spin systems (Figure 3, most intense spectrum). This effect and the associated distortion of the spectral lineshape can easily lead to misestimations of the ^{1}H polarization level.

The experimental linewidths of the ^{1}H echo-detected NMR spectra are dominated by intermolecular ^{1}H-^{1}H dipolar interaction. The current simulation reasonably accounts for this broadening contribution to the echo-based NMR linewidth, although the linewidth of the experimental spectrum at P_H = -75% is broader than that of the associated simulated spectrum. The simulation of the echo-based ^{1}H NMR spectrum also shows a minor discrepancy compared with the experimental lineshape towards the spectral baseline (see Figure 5). This discrepancy could be associated with sources of additional broadening, such as paramagnetic radical-induced nuclear spin relaxation, and inhomogeneous B_0- and B_1-fields.

It is worth noting that although the refocused ^{1}H NMR spectra are significantly narrower (~75 kHz) than those detected with a pulse-acquire experiment (~135 kHz), the relatively large linewidths of the ^{1}H NMR spectra hinder the efficiency of the echo-based approach due to the limited *rf*-pulse bandwidth. Nevertheless, in the current experiments, the Pake horns of the echo-based spectrum are observable. To improve the performance of this approach, the two Pake horns would have to be observed with much narrower linewidths. Isolated water molecules, such as those of $H_2O@C_{60}$ [25] or water-impregnated barium chlorate monohydrate [46], [47] provide a choice of possible candidate systems.

It is also interesting to note that a choice of t_{echo} = 30 μs led to minor peak distortions which were observable at lower levels of ^{1}H polarization and motivated the use of t_{echo} = 35 μs. Such distortions were not clearly observed at higher levels of P_H or for the case of t_{echo} = 40 μs. It is likely that radiation damping under microwave irradiation with negative DNP enhancements causes lengthening of the FID which needed to be accounted for in the echo-based experiments [48].

The use of an echo-based *rf*-pulse sequence offers a solution to alleviate the problem of spectral lineshape distortions (see Figures 4 and 5), since the approach can ultimately control the lineshape of the strongly hyperpolarized H_2O system to a considerably greater extent than a typical pulse-acquire experiment due to the echo compensation of the spectrometer dead time. However, a complication is the similarity between the lineshapes of the ^{1}H NMR spectra acquired over a range of ^{1}H spin polarization levels. Greater deviations over a smaller range of spin temperatures have been shown in the context of ^{2}H DNP thermometry [37]. Lineshape polarimetry has also proven to be an advantageous tool to measure the ^{15}N polarization of hyperpolarized $^{15}N_2O$ in the solid-state [49]. Indirect measurements of ^{1}H polarizations by using ^{13}C lineshape polarimetry of $^{13}CH_3$ groups has also been demonstrated [33]. Asymmetric ^{75}As NMR spectra were additionally observed from the interface region of single-crystal semi-insulating GaAs [50].

The above evidence is sufficient to argue that the dead time is the dominating effect which distorts the proton NMR lineshape at high levels of ^{1}H spin polarization (see Figure 3). However, other effects with potentially similar consequences should be briefly mentioned. (*i*) Possible variations of the transverse relaxation time T_2 across the Pake pattern. The ^{1}H NMR signal loss within the dead time would be dependent on the frequencies spanned by different parts of the spectrum, but can cause additional spectral artefacts only if T_2 is orientation dependent. A measurement of the transverse relaxation time constant T_2 is reported in the ESI, with $T_2 = 63.9 \pm 0.5$ μs [51]. This is considerably longer than the dead time employed in pulse-acquire experiments, but on the order of the echo time $2t_{echo}$ used in echo-based experiments and as a result T_2 relaxation reduces the intensity and also could potentially influence the lineshape of echo-based spectra, which could be related to some discrepancy between the experimental and simulated spectra shown in Figure 5, but is unlikely to influence those of the pulse-acquire measurements. (*ii*) The orientation dependence of the longitudinal relaxation time T_1, which has been explored for cases such as solid hydrates [46], [47]. Since the level of ^{1}H spin polarization depends on T_1, the orientational dependence of T_1 may lead to an orientation-dependent polarization level, which could potentially distort the lineshape of the observed ^{1}H NMR spectra. However, it can be safely stated that these effects, even if present, are not sufficiently large as to be observed in the presence of the dominating dead time-induced spectral distortion at high levels of ^{1}H spin polarization.

Such observations have only been made for hyperpolarized water at present. This is attributable to the presence of the strong ^{1}H-^{1}H dipolar coupling in H_2O, which manifests in the experimental spectrum. This phenomenon is unlikely to be clearly resolved in the hyperpolarized ^{1}H NMR spectra of other ^{1}H containing compounds relevant to *d*DNP since the ^{1}H spins within the DNP solvent also contribute to the NMR lineshape in a non-negligible manner and weaker ^{1}H-^{1}H/X dipolar couplings are typically present, which are not resolved in the ^{1}H NMR spectra of such glassy samples due to other linewidth dominating interactions, such as intramolecular dipolar couplings. Nevertheless, even if not easily recognizable, these effects may still be present in the DNP-enhanced NMR spectra of other molecules and may need to be accounted for in the data interpretation.

5. Conclusions

The ^{1}H NMR spectrum of water in a frozen glassy sample hyperpolarized under *d*DNP conditions has been shown to clearly deviate from the traditional Pake pattern acquired in high field and room temperature experiments [45], [46]. A greater than anticipated frequency splitting is observed between the two peaks of the Pake pattern, and their relative intensity seemingly indicates a misestimation of the ^{1}H spin polarization. Lineshape simulations indicate that NMR spectra recorded far from thermal equilibrium at high values of the proton spin polarization are distorted due to the emergence of an artificial peak, which occurs due to the influence of the spectrometer dead time and is unrelated to the smaller Pake horn. These pronounced distortions of the spectral lineshape and of the relative intensities of characteristic spectral features need to be fully understood and taken into account for a correct interpretation of data and an accurate evaluation of the level of spin polarization achieved in such *d*DNP experiments. We further demonstrated that such deleterious effects can be avoided by detecting two-pulse echo signals instead of a single-pulse FID. The echo-based NMR experiments were performed to mitigate the influence of the spectrometer dead time and lineshape simulations were used to precisely probe the level of ^{1}H spin polarization, inferring a ^{1}H polarization of -75% after ~34 minutes of microwave irradiation at the negative lobe of the DNP enhancement profile. This is advantageous since an accompanying thermal equilibrium reference spectrum is not required. These results are encouraging for future applications of experiments employing hyperpolarized water. As a side note, the ^{1}H NMR signal from hyperpolarized water could be used as a spy to accurately quantify the nuclear spin polarization of less abundant or residual protons present in the sample.

Acknowledgements

This research was supported by Claude Bernard University of Lyon 1, the ENS de Lyon, the French CNRS, and the European Research Council under the European Union's Horizon 2020 Research and Innovation Program (ERC Grant Agreement No. 714519 / HP4all and Marie Skłodowska-Curie Grant Agreement No. 766402 / ZULF). The authors gratefully acknowledge *Bruker Biospin* for providing the prototype *d*DNP polarizer, and particularly Dmitry Eshchenko, Roberto Melzi, Marc Rossire, Marco Sacher and James Kempf for scientific and technical support. The authors gratefully acknowledge Jasmine Viger-Gravel and Federico Paruzzo for enlightening discussions regarding *SIMPSON* simulations. IVK thanks the Russian Ministry of Science and Higher Education (State Contract No. 075-15-2021-580) for financial support.

References

[1] K. V. Kovtunov *et al.*, "Hyperpolarized NMR: d-DNP, PHIP, and SABRE," *Chem. Asian J.*, vol. 13, pp. 1857–1871, 2018, doi: 10.1002/asia.201800551.

[2] S. J. Elliott *et al.*, "Practical dissolution dynamic nuclear polarization," *Prog. Nucl. Magn. Reson. Spectrosc.*, vol. 126–127, pp. 59–100, 2021, doi: 10.1016/j.pnmrs.2021.04.002.

[3] J. H. Ardenkjaer-Larsen *et al.*, "Increase in signal-to-noise ratio of >10,000 times in liquid-state NMR," *Proc. Natl. Acad. Sci.*, vol. 100, pp. 10158–10163, 2003, doi: 10.1073/pnas.1733835100.

[4] J. H. Ardenkjaer-Larsen, "On the present and future of dissolution-DNP," *J. Magn. Reson.*, vol. 264, pp. 3–12, Mar. 2016, doi: 10.1016/j.jmr.2016.01.015.

[5] S. Jannin, J.-N. N. Dumez, P. Giraudeau, and D. Kurzbach, "Perspectives in Magnetic Resonance Application and methodology of dissolution dynamic nuclear polarization in physical, chemical and biological contexts," *J. Magn. Reson.*, vol. 305, pp. 41–50, 2019, doi: 10.1016/j.jmr.2019.06.001.

[6] Q. Chappuis *et al.*, "Hyperpolarized water to study protein-ligand interactions," *J. Phys. Chem. Lett.*, vol. 6, no. 9, pp. 1674–1678, 2015, doi: 10.1021/acs.jpclett.5b00403.

[7] B. T. Chung *et al.*, "First Hyperpolarized [2-13C]Pyruvate MR Studies of Human Brain Metabolism," *J. Magn. Reson.*, vol. 309, p. 106617, 2019, doi: 10.1016/j.jmr.2019.106617.

[8] S. J. Nelson *et al.*, "Metabolic imaging of patients with prostate cancer using hyperpolarized [1-13C]pyruvate," *Sci. Transl. Med.*, vol. 5, no. 198, p. 198ra108, 2013, doi: 10.1126/scitranslmed.3006070.

[9] J. Kurhanewicz *et al.*, "Hyperpolarized ^{13}C MRI: Path to Clinical Translation in Oncology," *Neoplasia (United States)*, vol. 21, pp. 1–16, 2019, doi: 10.1016/j.neo.2018.09.006.

[10] A. Abragam and M. Goldman, "Principles of dynamic nuclear polarisation," *Reports Prog. Phys.*, vol. 41, no. 3, pp. 395–467, 1978, doi: 10.1088/0034-4885/41/3/002.

[11] A. Pines, M. G. Gibby, and J. S. Waugh, "Proton-enhanced nuclear induction spectroscopy 13C chemical shielding anisotropy in some organic solids," *Chem. Phys. Lett.*, vol. 15, no. 3, pp. 373–376, 1972, doi: 10.1016/0009-2614(72)80191-X.

[12] S. R. Hartmann and E. L. Hahn, "Nuclear double resonance in the rotating frame," *Phys. Rev.*, vol. 128, no. 5, pp. 2042–2053, 1962, doi: 10.1103/PhysRev.128.2042.

[13] A. Bornet, R. Melzi, S. Jannin, and G. Bodenhausen, "Cross Polarization for Dissolution Dynamic Nuclear Polarization Experiments at Readily Accessible Temperatures $1.2 < T < 4.2$ K," *Appl. Magn. Reson.*, vol. 43, no. 1–2, pp. 107–117, 2012, doi: 10.1007/s00723-012-0358-1.

[14] A. Bornet and S. Jannin, "Optimizing dissolution dynamic nuclear polarization," *J. Magn. Reson.*, vol. 264, pp. 13–21, 2016, doi: 10.1016/j.jmr.2015.12.007.

[15] S. Jannin, A. Bornet, S. Colombo, and G. Bodenhausen, "Low-temperature cross polarization in view of enhancing dissolution Dynamic Nuclear Polarization in NMR," *Chem. Phys. Lett.*, vol. 517, no. 4–6, pp. 234–236, 2011, doi: 10.1016/j.cplett.2011.10.042.

[16] S. J. Elliott *et al.*, "Dipolar order mediated 1H→13C cross-polarization for dissolution-dynamic nuclear polarization," *Magn. Reson.*, vol. 1, pp. 89–96, 2020, doi: 10.5194/mr-1-89-2020.

[17] S. J. Elliott *et al.*, "Pulse sequence and sample formulation optimization for dipolar order mediated 1H→13C cross-polarization," *Phys. Chem. Chem. Phys.*, vol. 23, pp. 9457–9465, 2021, doi: 10.1039/d1cp00429h.

[18] S.J. Elliott et al., "Boosting Dissolution-Dynamic Nuclear Polarization by Multiple-Step Dipolar Order Mediated 1H→13C Cross-Polarization," *J. Magn. Reson. Open*, vol. 8–9, p. 10018, 2021, doi: https://doi.org/10.1016/j.jmro.2021.100018.

[19] S.J. Elliott et al., "Protonation Tuned Dipolar Order Mediated 1H→13C Cross-Polarization for Dissolution-Dynamic Nuclear Polarization Experiments," *Submitt. to Solid State Nucl. Magn. Reson.*, 2021.

[20] A. Sadet *et al.*, "Hyperpolarized Water Enhances Two-Dimensional Proton NMR Correlations: A New Approach for Molecular Interactions," *J. Am. Chem. Soc.*, 2019, doi: 10.1021/jacs.9b03651.

[21] M. Novakovic *et al.*, "A 300-fold enhancement of imino nucleic acid resonances by hyperpolarized water provides a new window for probing RNA refolding by 1D and 2D NMR," *Proc. Natl. Acad. Sci. U. S. A.*, vol. 117, no. 5, pp. 2449–2455, 2020, doi: 10.1073/pnas.1916956117.

[22] T. Harris, O. Szekely, and L. Frydman, "On the potential of hyperpolarized water in biomolecular NMR studies," *J. Phys. Chem. B*, vol. 118, no. 12, pp. 3281–3290, Mar. 2014, doi: 10.1021/jp4102916.

[23] K. L. Ivanov and G. Bodenhausen, "Generating para-water from para-hydrogen: A Gedankenexperiment," *J. Magn. Reson.*, vol. 292, pp. 48–52, 2018, doi: 10.1016/j.jmr.2018.05.003.

[24] C. R. Bowers and D. P. Weitekamp, "Parahydrogen and Synthesis Allow Dramatically Enhanced Nuclear Alignment," *J. Am. Chem. Soc.*, vol. 109, no. 18, pp. 5541–5542, 1987, doi: 10.1021/ja00252a049.

[25] B. Meier *et al.*, "Spin-Isomer Conversion of Water at Room Temperature and Quantum-Rotor-Induced Nuclear Polarization in the Water-Endofullerene H2O@C60," *Phys. Rev. Lett.*, vol. 120, p. 266001, 2018, doi: 10.1103/PhysRevLett.120.266001.

[26] G. Pileio, *Long-lived Nuclear Spin Order*. The Royal Society of Chemistry, 2020.
[27] D. Mammoli *et al.*, "Challenges in preparing, preserving and detecting para-water in bulk: overcoming proton exchange and other hurdles," *Phys. Chem. Chem. Phys.*, vol. 17, pp. 26819–26827, 2015, doi: 10.1039/c5cp03350k.
[28] A. Abragam, M. Chapellier, J. F. Jacquinot, and M. Goldman, "Absorption lineshape of highly polarized nuclear spin systems," *J. Magn. Reson.*, vol. 10, pp. 322–346, 1973, doi: 10.1016/0022-2364(73)90253-9.
[29] C. M. Edwards, D. Zhou, and N. S. Sullivan, "Unusual low-temperature effects on the NMR line shapes in solid hydrogen," *Phys. Rev. B*, vol. 43, pp. 6540–6542, 1986, doi: 10.1097/00042560-200105010-00007.
[30] R. N. Havemeyer, "Freezing Point Curve of Dimethyl Sulfoxide-Water Solutions," *J. Phamceutical Sci.*, vol. 55, pp. 851–853, 1966.
[31] S.J. Elliott et al., "In Preparation," 2021.
[32] A. Bornet, J. Milani, B. Vuichoud, A. J. Perez Linde, G. Bodenhausen, and S. Jannin, "Microwave frequency modulation to enhance Dissolution Dynamic Nuclear Polarization Dedicated to To Martial Rey, as a token of appreciation.," *Chem. Phys. Lett.*, vol. 602, pp. 63–67, 2014, doi: 10.1016/j.cplett.2014.04.013.
[33] S. J. Elliott, Q. Stern, and S. Jannin, "Solid-State 1H Spin Polarimetry by 13CH3 Nuclear Magnetic Resonance," *Magn. Reson. Discuss.*, vol. 2, pp. 643–652, 2021, doi: https://doi.org/10.5194/mr-2021-25.
[34] J. A. Marohn, P. J. Carson, J. Y. Hwang, M. A. Miller, D. N. Shykind, and D. P. Weitekamp, "Optical Larmor Beat Detection of High-Resolution Nuclear Magnetic Resonance in a Semiconductor Heterostructure," *Phys. Rev. Lett.*, vol. 75, pp. 1364–1367, Aug. 1995, doi: 10.1103/PhysRevLett.75.1364.
[35] S. Schäublin, A. Höhener, and R. R. Ernst, "Fourier spectroscopy of nonequilibrium states, application to CIDNP, overhauser experiments and relaxation time measurements," *J. Magn. Reson.*, vol. 13, pp. 196–216, 1974, doi: 10.1016/0022-2364(74)90007-9.
[36] J. S. Waugh, O. Gonen, and P. Kuhns, "Fourier transform NMR at low temperatures," *J. Chem. Phys.*, vol. 86, pp. 3816–3818, 1987, doi: 10.1063/1.451940.
[37] B. Aghelnejad, S. Marhabaie, M. Baudin, and G. Bodenhausen, "Spin Thermometry: A Straightforward Measure of Millikelvin Deuterium Spin Temperatures Achieved by Dynamic Nuclear Polarization," vol. 11, pp. 3219–3225, 2020, doi: 10.1021/acs.jpclett.0c00713.
[38] P. Kuhns, O. Gonen, and J. S. Waugh, "Proton spin-spin and spin-lattice relaxation in CaSO4 · xH2O below 1 K," *J. Magn. Reson.*, vol. 82, pp. 231–237, 1989, doi: 10.1016/0022-2364(89)90027-9.
[39] S. Chinthalapalli, A. Bornet, D. Carnevale, S. Jannin, and G. Bodenhausen, "Homonuclear decoupling for spectral simplification of carbon-13 enriched molecules in solution-state NMR enhanced by dissolution DNP," *Phys. Chem. Chem. Phys.*, vol. 18, pp. 11480–11487, 2016, doi: 10.1039/c5cp07884a.
[40] D. Carnevale, P. Pelupessy, and G. Bodenhausen, "Cross-term Splittings Due to the Orientational Inequivalence of Proton Magnetic Shielding Tensors: Do Water Molecules Trapped in Crystals Hop or Tunnel?," *J. Phys. Chem. Lett.*, vol. 10, pp. 3224–3231, Jun. 2019, doi: 10.1021/acs.jpclett.9b00914.
[41] X. Lu *et al.*, "Broadband excitation in solid-state NMR using interleaved DANTE pulse trains with N pulses per rotor period," *J. Magn. Reson.*, vol. 236, pp. 105–116, 2013, doi: 10.1016/j.jmr.2013.09.003.
[42] D. Carnevale, A. J. Perez Linde, G. Bauer, and G. Bodenhausen, "Solid-state proton NMR of paramagnetic metal complexes: DANTE spin echoes for selective excitation in inhomogeneously broadened lines," *Chem. Phys. Lett.*, vol. 580, pp. 172–178, 2013, doi: 10.1016/j.cplett.2013.06.052.
[43] M. Bak, J. T. Rasmussen, and N. C. Nielsen, "SIMPSON: a general simulation program for solid-state NMR spectroscopy. 2000.," *J. Magn. Reson.*, vol. 213, pp. 366–400, 2011, doi: 10.1016/j.jmr.2011.09.008.
[44] M. Edén and M. H. Levitt, "Computation of Orientational Averages in Solid-State NMR by Gaussian Spherical Quadrature," *J. Magn. Reson.*, vol. 132, pp. 220–239, 1998, doi: https://doi.org/10.1006/jmre.1998.1427.
[45] R. Freeman and J. Keeler, "Suppression of artifacts in two-dimensional J spectra," *J. Magn. Reson.*, vol. 43, pp. 484–487, 1981, doi: 10.1016/0022-2364(81)90061-5.
[46] D. Carnevale, S. E. Ashbrook, and G. Bodenhausen, "Solid-state NMR measurements and DFT calculations of the magnetic shielding tensors of protons of water trapped in barium chlorate monohydrate," *RSC Adv.*, vol. 4, pp. 56248–56258, 2014, doi: 10.1039/c4ra09992c.
[47] D. Carnevale, S. Marhabaie, P. Pelupessy, and G. Bodenhausen, "Orientation-Dependent Proton Relaxation of Water Molecules Trapped in Solids: Crystallites with Long-Lived Magnetization," *J. Phys. Chem. A*, vol. 123, pp. 9763–9769, 2019, doi: 10.1021/acs.jpca.9b07303.
[48] V. V. Krishnan and N. Murali, "Radiation damping in modern NMR experiments: Progress and challenges," *Prog. Nucl. Magn. Reson. Spectrosc.*, vol. 68, pp. 41–57, 2013, doi: 10.1016/j.pnmrs.2012.06.001.
[49] N. N. Kuzma *et al.*, "Lineshape-based polarimetry of dynamically-polarized 15N2O in solid-state mixtures," *J. Magn. Reson.*, vol. 234, pp. 90–94, 2013, doi: 10.1038/jid.2014.371.
[50] M. M. Willmering, Z. L. Ma, M. A. Jenkins, J. F. Conley, and S. E. Hayes, "Enhanced NMR with Optical Pumping Yields 75As Signals Selectively from a Buried GaAs Interface," *J. Am. Chem. Soc.*, vol. 139, pp. 3930–3933, 2017, doi: 10.1021/jacs.6b08970.
[51] N. S. Sullivan and R. V. Pound, "Nuclear-Spin-Lattice Relaxation of Solid Hydrogen at Low Temperatures," *Phys. Rev. A.*, vol. 6, pp. 1102–1107, 1972, doi: 10.1017/CBO9781107415324.004.